Effects of state dependent correlations on nucleon density and momentum distributions

F. Arias de Saavedra
Departamento de Fisica Moderna, Universidad de Granada, E-18071 Granada, Spain

G. Co' and M. M. Renis
Dipartimento di Fisica, Università di Lecce and INFN, Sezione di Lecce, I-73100 Lecce, Italy

(Received 1 May 1996)

The proton momentum and density distributions of closed shell nuclei are calculated with a model treating short-range correlations up to first order in the cluster expansion. The validity of the model is verified by comparing the results obtained using purely scalar correlations with those produced by finite nuclei Fermi hypernetted chain calculations. State dependent correlations are used to calculate momentum and density distributions of ^{12}C, ^{16}O, ^{40}Ca, and ^{48}Ca, and the effects of their tensor components are studied. [S0556-2813(97)02901-4]

PACS number(s): 21.10.Ft, 21.60.−n

I. INTRODUCTION

The high precision data produced by modern electron scattering experiments have imposed severe constraints on the validity of the models and the theories aiming to describe the nuclear properties. Since the beginning of the 1980s, elastic scattering experiments [1], measuring charge distributions, and knockout experiments [2], measuring spectral functions, have pointed out the difficulties of the mean-field model in the description of the ground state of atomic nuclei.

The effects not considered in the mean-field model have been generically named correlations. One usually distinguishes between short- and long-range correlations. The former ones are those acting at short interparticle distances modifying the mean-field single-particle wave functions to take care of the hard core part of the nuclear potential. The long-range correlations are instead acting on the full system and are produced by collective phenomena like sound waves or surface vibrations.

The correlated basis function (CBF) theory, based on Jastrow's approach [3], is particularly suitable for the study of the short-range correlations, since these correlations are explicitly included in the definition of the many-body wave function. Unfortunately the technical complexity of this theory has limited its application to few-body systems and to infinite nuclear matter [4–6]. At present there are only few examples of CBF calculations in nuclei heavier than ^{4}He. The CBF theory has been used in variational Monte Carlo calculations of the ^{16}O nucleus [7]. Only recently the Fermi hypernetted chain theory (FHNC) has been extended to describe the ground-state properties of medium-heavy doubly closed shell nuclei [8–10]. Unfortunately these calculations are still limited to the use of central interactions and scalar correlations.

Because of these difficulties, the study of short-range correlations in medium-heavy nuclei has been done using simplified models. Nuclear models considering short-range correlations have been used to analyze elastic electron scattering data already at the end of the 1960s [11]. These models are based on cluster expansion like the CBF theory, but they retain only those terms containing a single correlation line [12]. The truncation of the expansion simplifies the calculations and it is done in a way to conserve the normalization of the density distribution. More recently, these simplified models have been used to investigate also the nucleon momentum distributions [13–15].

The aim of the present work is twofold: first we would like to discuss the validity of these nuclear models, and second we would like to investigate the effects of the state dependent part of the correlation on density and momentum distributions.

For these purposes we extend the model developed in Ref. [16] to calculate both density and momentum distributions for doubly closed shell nuclei and we compare our results with those of finite nuclei FHNC calculations [10]. After this test, using a nuclear matter correlation function [17], we study the effects produced by the state dependent terms of the correlation on the proton density and the momentum distributions of the ^{12}C, ^{16}O, ^{40}Ca, and ^{48}Ca nuclei.

II. THE MODEL

The basic quantity of interest for our calculations is the one-body density matrix (OBDM) defined as

$$\rho(\mathbf{r}_1,\mathbf{r}_1') = \frac{A}{\mathcal{N}} \int d^3r_2\, d^3r_3 \cdots d^3r_A \times \Psi^\dagger(\mathbf{r}_1,\mathbf{r}_2,\mathbf{r}_3,\ldots,\mathbf{r}_A)\Psi(\mathbf{r}_1',\mathbf{r}_2,\mathbf{r}_3,\ldots,\mathbf{r}_A), \tag{1}$$

where Ψ is the nuclear ground-state wave function and $\mathcal{N} = \langle\Psi|\Psi\rangle$. In Eq. (1) a sum on the spin and isospin components of all the particles, particle 1 included, is understood.

In our model the protons and the neutrons are separately treated, therefore:

$$\rho(\mathbf{r}_1,\mathbf{r}_1') = \rho^p(\mathbf{r}_1,\mathbf{r}_1') + \rho^n(\mathbf{r}_1,\mathbf{r}_1'), \tag{2}$$

where the proton and neutron OBDM's are obtained inserting in Eq. (1) the operators selecting the protons

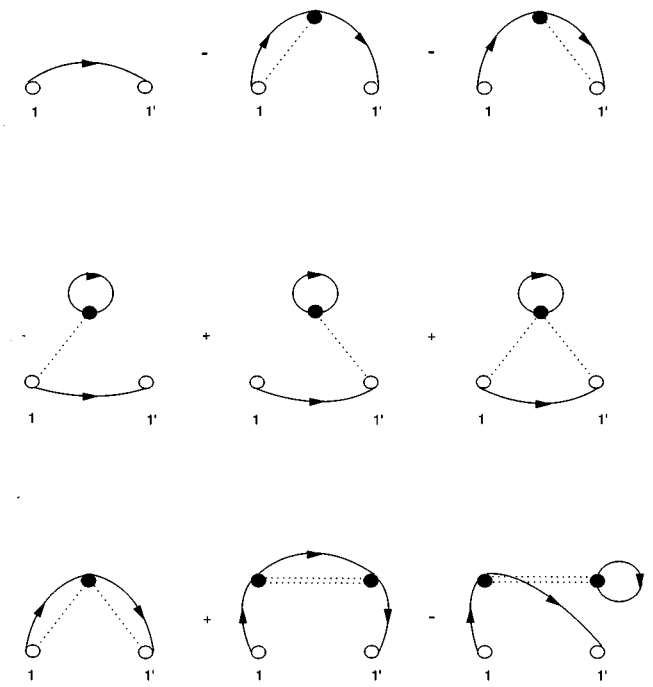

FIG. 1. Set of diagrams considered in our model. The oriented lines represent the uncorrelated OBDM [Eq. (10)] and the dotted lines represent the correlation functions h_n [Eq. (12)].

$$Q(1)=\frac{1}{2}[1+\tau_3(1)], \tag{3}$$

and the neutrons $1-Q(1)$.

The density distribution is the diagonal part of the OBDM ($\mathbf{r}_1=\mathbf{r}_1'$) while the momentum distribution is its Fourier transform:

$$n(\mathbf{k})=\frac{1}{A}\int d^3r_1 \int d^3r_1'\rho(\mathbf{r}_1,\mathbf{r}_1')e^{i\mathbf{k}\cdot(\mathbf{r}_1-\mathbf{r}_1')}. \tag{4}$$

The OBDM is normalized as

$$\int d^3r_1 \int d^3r_1'\rho(\mathbf{r}_1,\mathbf{r}_1')\,\delta(\mathbf{r}_1-\mathbf{r}_1')=A \tag{5}$$

and therefore

$$\int d^3k\; n(\mathbf{k})=(2\pi)^3. \tag{6}$$

Our model is based upon the Jastrow ansatz on the nuclear wave function [3]:

$$\Psi(1,\ldots,A)=F(1,\ldots,A)\Phi(1,\ldots,A), \tag{7}$$

where F is an A-body correlation operator, and Φ is a Slater determinant built on a basis of single-particle (s.p.) wave functions generated by a one-body Hamiltonian.

In the present work we shall use a spherical mean-field potential with a spin-orbit interaction, therefore the quantum numbers characterizing the s.p. wave functions are the principal quantum number n, the orbital angular momentum l, the total angular momentum j, its third component m, and the third isospin component t.

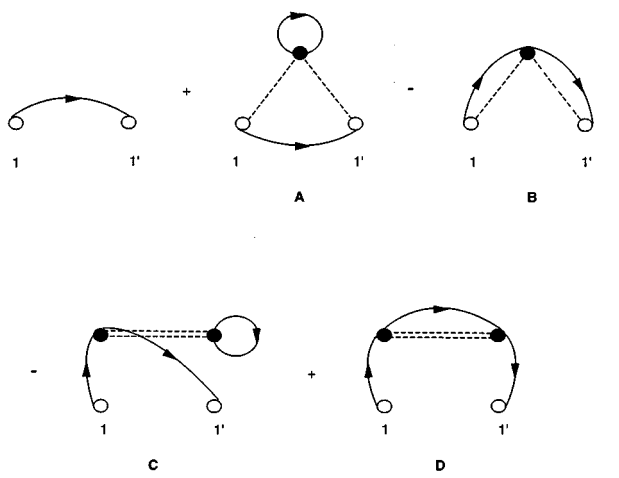

FIG. 2. Set of diagrams considered in our model. This set of diagrams corresponds to that of Fig. 1. In this figure the dashed lines indicate the dynamical correlations f_n [Eq. (8)].

A usual choice of the expression of the correlation operator is based upon an extension of the original Jastrow ansatz to a state dependent form:

$$F(1,\ldots,A)=S\prod_{j>i=1}^{A}\left(\sum_{n=1}^{M} f_n(r_{ij})O_{ij}^n\right), \tag{8}$$

where $r_{ij}=|\mathbf{r}_i-\mathbf{r}_j|$, and we have indicated with S a symmetrizer operator, with M the maximum number of the correlation channels and with O_{ij}^n the operators characterizing the various channels. In the present work we use correlations with six active channels defined as: $O_{ij}^1=1$, $O_{ij}^2=\boldsymbol{\sigma}(i)\cdot\boldsymbol{\sigma}(j)$, $O_{ij}^3=\boldsymbol{\tau}(i)\cdot\boldsymbol{\tau}(j)$, $O_{ij}^4=\boldsymbol{\sigma}(i)\cdot\boldsymbol{\sigma}(j)\boldsymbol{\tau}(i)\cdot\boldsymbol{\tau}(j)$, $O_{ij}^5=S_{ij}$, $O_{ij}^6=S_{ij}\boldsymbol{\tau}(i)\cdot\boldsymbol{\tau}(j)$, where S_{ij} is the tensor operator:

$$S_{ij}=3\frac{[\boldsymbol{\sigma}(i)\cdot\mathbf{r}_{ij}][\boldsymbol{\sigma}(j)\cdot\mathbf{r}_{ij}]}{(r_{ij})^2}-\boldsymbol{\sigma}(i)\cdot\boldsymbol{\sigma}(j). \tag{9}$$

The OBDM is calculated with cluster expansion techniques applied to finite systems [18]. We express the correlation function as

$$F(1,\ldots,A)=1+S\prod_{j>i=1}^{A}\left(\sum_{n=1}^{M} h_n(r_{ij})O_{ij}^n\right), \tag{10}$$

and perform the expansion in terms of h_n.

The denominator in Eq. (1) cancels all the unlinked diagrams of the numerator, i.e., all the diagrams which do not have a direct link, either statistical or dynamical one, with the points $\mathbf{r}$ and $\mathbf{r}'$.

The basic hypothesis of the model enters now, because of all the infinite set of linked diagrams obtained within the cluster expansion, we retain only those containing correlations lines up to the second order in the correlation function h_n. The set of diagrams considered is shown in Fig. 1. This is the lowest order set of correlated diagrams conserving the normalization of the OBDM, Eq. (5).

It is possible to describe this limited set of diagrams in terms of the correlation function f_n. In this new representation the set of diagrams to be calculated is shown in Fig. 2.

The OBDM calculated with the diagrams of Fig. 2 can be expressed as

$$\begin{aligned}\rho_1^p(\mathbf{r}_1,\mathbf{r}_1') &\equiv \rho_0^p(\mathbf{r}_1,\mathbf{r}_1')+A(\mathbf{r}_1,\mathbf{r}_1')-B(\mathbf{r}_1,\mathbf{r}_1')-C(\mathbf{r}_1,\mathbf{r}_1')+D(\mathbf{r}_1,\mathbf{r}_1') \\ &= \rho_0^p(\mathbf{r}_1,\mathbf{r}_1')+\rho_0(\mathbf{r}_1,\mathbf{r}_1')\int d^3r_2 \;\; H(\mathbf{r}_1,\mathbf{r}_1',\mathbf{r}_2)\rho_0(\mathbf{r}_2,\mathbf{r}_2)-\int d^3r_2\rho_0(\mathbf{r}_1,\mathbf{r}_2) \;\; H(\mathbf{r}_1,\mathbf{r}_1',\mathbf{r}_2)\rho_0(\mathbf{r}_2,\mathbf{r}_1') \\ &\quad -\int d^3r_2\int d^3r_3\rho_0(\mathbf{r}_1,\mathbf{r}_2)\rho_0(\mathbf{r}_2,\mathbf{r}_1')\rho_0(\mathbf{r}_3,\mathbf{r}_3) \;\; H(\mathbf{r}_2,\mathbf{r}_2,\mathbf{r}_3) \\ &\quad +\int d^3r_2\int d^3r_3\rho_0(\mathbf{r}_1,\mathbf{r}_2)\rho_0(\mathbf{r}_2,\mathbf{r}_3)\rho_0(\mathbf{r}_3,\mathbf{r}_1') \;\; H(\mathbf{r}_2,\mathbf{r}_2,\mathbf{r}_3), \end{aligned} \tag{11}$$

where, as in Eq. (1), the sum on spin and isospin components is understood.

In the above expression we have used the uncorrelated OBDM defined in terms of the s.p. wave functions as

$$\rho_0(\mathbf{r}_1,\mathbf{r}_2)=\sum_{nljmt}\phi^{*t}_{nljm}(\mathbf{r}_1)\phi^{t}_{nljm}(\mathbf{r}_2). \tag{12}$$

In the diagrams of Fig. 2 the $\rho_0(\mathbf{r}_1,\mathbf{r}_2)$ is represented by an oriented line. The dashed lines represent the dynamical correlations expressed in Eq. (11) by the coefficients $H(\mathbf{r}_1,\mathbf{r}_2,\mathbf{r}_3)$ defined as

$$H(\mathbf{r}_1,\mathbf{r}_2,\mathbf{r}_3)=\left(\sum_{p=1}^{6} f_p(r_{13})O^p_{13}\right)Q(1)\left(\sum_{q=1}^{6} f_q(r_{23})O^q_{13}\right), \tag{13}$$

with $Q(1)$ defined by Eq. (3).

It is easy to see that the set of considered diagrams conserves the density normalization. Because of the property of the uncorrelated density

$$\int d^3r_j \;\; \rho_0(\mathbf{r}_i,\mathbf{r}_j)\rho_0(\mathbf{r}_j,\mathbf{r}_k)=\rho_0(\mathbf{r}_i,\mathbf{r}_k), \tag{14}$$

where we have also summed on the spin and isospin coordinates of the particle j, we obtain the following relations among the diagrams of Fig. 2:

$$\int d^3r_1\int d^3r_1' \;\; A(\mathbf{r}_1,\mathbf{r}_1') \;\; \delta(\mathbf{r}_1-\mathbf{r}_1') = \int d^3r_1\int d^3r_1' \;\; C(\mathbf{r}_1,\mathbf{r}_1') \;\; \delta(\mathbf{r}_1-\mathbf{r}_1'), \tag{15}$$

$$\int d^3r_1\int d^3r_1' \;\; B(\mathbf{r}_1,\mathbf{r}_1') \;\; \delta(\mathbf{r}_1-\mathbf{r}_1') = \int d^3r_1\int d^3r_1' \;\; D(\mathbf{r}_1,\mathbf{r}_1') \;\; \delta(\mathbf{r}_1-\mathbf{r}_1') \tag{16}$$

and therefore

$$\int d^3r_1\int d^3r_1' \;\; \rho_1^p(\mathbf{r}_1,\mathbf{r}_1') \;\; \delta(\mathbf{r}_1-\mathbf{r}_1') = \int d^3r_1\int d^3r_1' \;\; \rho_0^p(\mathbf{r}_1,\mathbf{r}_1') \;\; \delta(\mathbf{r}_1-\mathbf{r}_1')=Z. \tag{17}$$

In the evaluation of the spin and isospin traces of the correlation kernels of Eq. (13), we found it convenient to separate the various terms with respect to their isospin dependence and we obtain four terms:

$$\begin{aligned} H(\mathbf{r}_1,\mathbf{r}_1',\mathbf{r}_2) &= [f_1g_1+3f_2g_2+6f_5g_5+(f_1g_2+f_2g_1-2f_2g_2+2f_5g_5)\boldsymbol{\sigma}(1)\cdot\boldsymbol{\sigma}(2)+(f_1g_5+f_5g_1+f_2g_5+f_5g_2 \\ &\quad -2f_5g_5)S_{12}]Q(1) \\ &\quad +[f_3g_1+3f_4g_2+6f_6g_5+(f_3g_2+f_4g_1-2f_4g_2+2f_6g_5)\boldsymbol{\sigma}(1)\cdot\boldsymbol{\sigma}(2)+(f_3g_5+f_6g_1+f_4g_5 \\ &\quad +f_6g_2-2f_6g_5)S_{12}]\boldsymbol{\tau}(1)\cdot\boldsymbol{\tau}(2)Q(1) \\ &\quad +[f_1g_3+3f_2g_4+6f_5g_6+(f_1g_4+f_2g_3-2f_2g_4+2f_5g_6)\boldsymbol{\sigma}(1)\cdot\boldsymbol{\sigma}(2) \\ &\quad +(f_1g_6+f_5g_3+f_2g_6+f_5g_4-2f_5g_6)S_{12}]Q(1)\boldsymbol{\tau}(1)\cdot\boldsymbol{\tau}(2) \\ &\quad +[f_3g_3+3f_4g_4+6f_6g_6+(f_3g_4+f_4g_3-2f_4g_4+2f_6g_6)\boldsymbol{\sigma}(1)\cdot\boldsymbol{\sigma}(2)+(f_3g_6+f_6g_3+f_4g_6+f_6g_4 \\ &\quad -2f_6g_6)S_{12}]\boldsymbol{\tau}(1)\cdot\boldsymbol{\tau}(2)Q(1)\boldsymbol{\tau}(1)\cdot\boldsymbol{\tau}(2). \end{aligned} \tag{18}$$

TABLE I. Isospin traces of Eq. (18) for each diagram considered.

	A	C
$\langle Q(1)\rangle$	$\delta_{t1,p}$	$\delta_{t1,p}\delta_{t2,p}$
$\langle \boldsymbol{\tau}(1)\cdot\boldsymbol{\tau}(2)Q(1)\rangle$	$\delta_{t1,p}(2\delta_{t2,p}-1)$	$\delta_{t1,p}\delta_{t2,p}(2\delta_{t3,p}-1)$
$\langle Q(1)\boldsymbol{\tau}(1)\cdot\boldsymbol{\tau}(2)\rangle$	$\delta_{t1,p}(2\delta_{t2,p}-1)$	$\delta_{t1,p}\delta_{t2,p}(2\delta_{t3,p}-1)$
$\langle \boldsymbol{\tau}(1)\cdot\boldsymbol{\tau}(2)Q(1)\boldsymbol{\tau}(1)\cdot\boldsymbol{\tau}(2)\rangle$	$(2\delta_{t2,p}-\delta_{t1,p})^2$	$\delta_{t1,p}\delta_{t2,p}(5-4\delta_{t3,p})$
	B	D
$\langle Q(1)\rangle$	$\delta_{t1,p}\delta_{t2,p}$	$\delta_{t1,p}\delta_{t2,p}\delta_{t3,p}$
$\langle \boldsymbol{\tau}(1)\cdot\boldsymbol{\tau}(2)Q(1)\rangle$	$\delta_{t1,p}(2-\delta_{t2,p})$	$\delta_{t1,p}\delta_{t3,p}(2-\delta_{t2,p})$
$\langle Q(1)\boldsymbol{\tau}(1)\cdot\boldsymbol{\tau}(2)\rangle$	$\delta_{t2,p}(2-\delta_{t1,p})$	$\delta_{t1,p}\delta_{t3,p}(2-\delta_{t2,p})$
$\langle \boldsymbol{\tau}(1)\cdot\boldsymbol{\tau}(2)Q(1)\boldsymbol{\tau}(1)\cdot\boldsymbol{\tau}(2)\rangle$	$5\delta_{t1,p}\delta_{t2,p}-2\delta_{t1,p}-2\delta_{t2,p}$	$\delta_{t1,p}\delta_{t3,p}(5\delta_{t2,p}-4)$

In the above expression to simplify the writing, we used the symbol f_n for the correlation functions depending from $\mathbf{r}_1$ and $\mathbf{r}_2$, and g_n for those depending from $\mathbf{r}_1'$ and $\mathbf{r}_2$. Clearly, in the case $\mathbf{r}_1=\mathbf{r}_1'$ we have $f_n=g_n$.

The calculation continues inserting the above expression in Eq. (11) and evaluating the spin and isospin traces. The traces of the isospin dependent part of each term are given in Table I. We have explicitly verified that the spin traces of all the terms depending from the tensor operator are zero. This is due to the definition of the tensor operator, Eq. (9), to the spherical symmetry of the problem, and to the saturation of the spin of all the single-particle wave functions.

In order to express the final result we used the quantity $\rho_0^{s1,s2,t}(\mathbf{r}_1,\mathbf{r}_2)$ defined by the relation

$$\rho_0(\mathbf{r}_1,\mathbf{r}_2)=\sum_{t=p,n}\sum_{s1s2}\rho_0^{s1,s2,t}(\mathbf{r}_1,\mathbf{r}_2)\chi_{s1}^{\dagger}(1)\chi_{s2}(2)\chi_t^{\dagger}(1)\chi_t(2), \tag{19}$$

where we have indicated with χ the spin and isospin wave functions. Together with the above definition we define as well

$$\rho_0^t(\mathbf{r}_1,\mathbf{r}_2)=\sum_s \rho_0^{s,s,t}(\mathbf{r}_1,\mathbf{r}_2), \tag{20}$$

$$\rho_0^t(\mathbf{r}_1)=\rho_0^t(\mathbf{r}_1,\mathbf{r}_1). \tag{21}$$

Using the quantities defined above we express the four terms composing ρ_1^p, Eq. (11), as

$$A(\mathbf{r}_1,\mathbf{r}_1')=\rho_0^p(\mathbf{r}_1,\mathbf{r}_1')\int d^3r_2[\rho_0^p(\mathbf{r}_2)G1(\mathbf{r}_1,\mathbf{r}_1',\mathbf{r}_2)+\rho_0^n(\mathbf{r}_2)G2(\mathbf{r}_1,\mathbf{r}_1',\mathbf{r}_2)]+4\rho_0^n(\mathbf{r}_1,\mathbf{r}_1')\int d^3r_2\rho_0^p(\mathbf{r}_2)G3(\mathbf{r}_1,\mathbf{r}_1',\mathbf{r}_2), \tag{22}$$

$$\begin{aligned}B(\mathbf{r}_1,\mathbf{r}_1')=\int d^3r_2\Bigg\{&\sum_{s1\,s2}\rho_0^{s1,s2,p}(\mathbf{r}_1,\mathbf{r}_2)\rho_0^{s2,s1,p}(\mathbf{r}_2,\mathbf{r}_1')\;\; G4(\mathbf{r}_1,\mathbf{r}_1',\mathbf{r}_2)+2\rho_0^p(\mathbf{r}_1,\mathbf{r}_2)\rho_0^p(\mathbf{r}_2,\mathbf{r}_1')\;\; G5(\mathbf{r}_1,\mathbf{r}_1',\mathbf{r}_2)\\&+\sum_{s1\,s2}2\rho_0^{s1,s2,p}(\mathbf{r}_1,\mathbf{r}_2)\rho_0^{s2,s1,n}(\mathbf{r}_2,\mathbf{r}_1')\;\; G6(\mathbf{r}_1,\mathbf{r}_1',\mathbf{r}_2)+4\rho_0^p(\mathbf{r}_1,\mathbf{r}_2)\rho_0^n(\mathbf{r}_2,\mathbf{r}_1')\;\; G7(\mathbf{r}_1,\mathbf{r}_1',\mathbf{r}_2)\\&+\sum_{s1\,s2}2\rho_0^{s1,s2,n}(\mathbf{r}_1,\mathbf{r}_2)\rho_0^{s2,s1,p}(\mathbf{r}_2,\mathbf{r}_1')\;\; G8(\mathbf{r}_1,\mathbf{r}_1',\mathbf{r}_2)+4\rho_0^n(\mathbf{r}_1,\mathbf{r}_2)\rho_0^p(\mathbf{r}_2,\mathbf{r}_1')\;\; G9(\mathbf{r}_1,\mathbf{r}_1',\mathbf{r}_2)\Bigg\},\end{aligned} \tag{23}$$

$$\begin{aligned}C(\mathbf{r}_1,\mathbf{r}_1')=\int d^3r_2\int d^3r_3\sum_{s1\,s2}&\rho_0^{s1,s2,p}(\mathbf{r}_1,\mathbf{r}_2)\rho_0^{s2,s1,p}(\mathbf{r}_2,\mathbf{r}_1')\;\; \{\rho_0^p(\mathbf{r}_3)G1(\mathbf{r}_2,\mathbf{r}_2,\mathbf{r}_3)+\rho_0^n(\mathbf{r}_3)[G2(\mathbf{r}_2,\mathbf{r}_2,\mathbf{r}_3)\\&+4G3(\mathbf{r}_2,\mathbf{r}_2,\mathbf{r}_3)]\},\end{aligned} \tag{24}$$

$$\begin{aligned}D(\mathbf{r}_1,\mathbf{r}_1')=\int d^3r_2\int d^3r_3\Bigg(&\sum_{s1\,s2\,s3}\rho_0^{s1,s2,p}(\mathbf{r}_1,\mathbf{r}_2)\rho_0^{s3,s1,p}(\mathbf{r}_3,\mathbf{r}_1')\;\; \{\rho_0^{s2,s3,p}(\mathbf{r}_2,\mathbf{r}_3)G4(\mathbf{r}_2,\mathbf{r}_2,\mathbf{r}_3)+2\rho_0^{s2,s3,n}(\mathbf{r}_2,\mathbf{r}_3)[G6(\mathbf{r}_2,\mathbf{r}_2,\mathbf{r}_3)\\&+G8(\mathbf{r}_2,\mathbf{r}_2,\mathbf{r}_3)]\}+\sum_{s1\,s2}\rho_0^{s1,s2,p}(\mathbf{r}_1,\mathbf{r}_2)\rho_0^{s2,s1,p}(\mathbf{r}_3,\mathbf{r}_1')2\{\rho_0^p(\mathbf{r}_2,\mathbf{r}_3)G5(\mathbf{r}_2,\mathbf{r}_2,\mathbf{r}_3)+2\rho_0^n(\mathbf{r}_2,\mathbf{r}_3)[G7(\mathbf{r}_2,\mathbf{r}_2,\mathbf{r}_3)\\&+G9(\mathbf{r}_2,\mathbf{r}_2,\mathbf{r}_3)]\}\Bigg).\end{aligned} \tag{25}$$

The explicit expression of the terms G containing the correlation functions are given in the Appendix.

The calculation of the momentum and density distributions of doubly magic nuclei has been done by exploiting the spherical symmetry of the problem to perform an analytical integration on the angular variables. For this purpose we have expressed the s.p. wave functions in spherical coordinates and we have performed a multipole expansion of the functions G containing the correlations. In the Appendix we present the basic points of the calculation and we give the final expressions used to evaluate the diagrams A, B, C, and D. The details of the calculation are presented in Ref. [19].

III. RESULTS

In our calculations the s.p. wave functions have been generated by a spherical Woods-Saxon well of the form:

$$V(\mathbf{r}) = \frac{-V_0}{1+e^{(r-R)/a}} + \left(\frac{\hbar}{m_\pi c}\right)^2 \frac{1}{r}\frac{d}{dr}\left(\frac{-V_{ls}}{1+e^{(r-R)/a}}\right) \boldsymbol{l}\cdot\boldsymbol{\sigma} + V_{\mathrm{Coul}}, \qquad (26)$$

where m_π is the pion mass.

For each nucleus considered, we have taken from the literature [20] the parameters of the potential (see Table II). These parameters have been fixed to reproduce the s.p. energies around the Fermi surface and the root mean squared charge radii.

We tested the validity of our model by comparing our results with those of FHNC calculations performed with the same inputs. We used two kinds of correlation functions. A first one has a Gaussian functional dependence from the interparticle distance. The second one has been obtained in Ref. [10] by solving the variational equations for the mean value of the Hamiltonian up to the second order (Euler correlations).

The correlations used for the ^{12}C and ^{48}Ca nuclei are shown in Fig. 3. The dashed lines represent the Gaussian correlations, while the full lines show the Euler correlations. These correlations have been fixed in Ref. [10] by minimizing the nuclear binding energies for the Afnan and Tang S3 interaction [21]. The Euler correlations show an overshooting of the asymptotic value in the region between 1 and 2 fm.

TABLE II. Coefficients of the Woods-Saxon potential Eq. (26).

		V_0	V_{LS}	R	a
^{12}C	p	62.00	3.20	2.86	0.57
	n	60.00	3.15	2.86	0.57
^{16}O	p	52.50	7.00	3.20	0.53
	n	52.50	6.54	3.20	0.53
^{40}Ca	p	57.50	11.11	4.10	0.53
	n	55.00	8.50	4.10	0.53
^{48}Ca	p	59.50	8.55	4.36	0.53
	n	50.00	7.74	4.36	0.53

In Fig. 4 we compare the momentum and density distributions calculated within the FHNC theory [10] (dashed lines) and those obtained with the present model (full lines). The agreement between the two calculations is quite good, independently from the correlation function used.

Confident of the validity of our model we use the nuclear matter state dependent correlation function of Ref. [17] to calculate momentum and density distributions in ^{12}C, ^{16}O, ^{40}Ca, and ^{48}Ca.

We show in Fig. 5 the various terms of the correlation as a function of the interparticle distance. The dominant term of the correlation is the scalar channel. The tensor term (f_5) is extremely small and the tensor-isospin term (f_6) is peaked at an interparticle distance of about 1 fm.

In Figs. 6 and 7 we show the proton density and momentum distributions for the four nuclei considered calculated by switching on and off the various channels of the correlation function. The dotted lines represent the uncorrelated results. The results of the calculations performed with the correlation containing all the six channels are shown by the full lines. The dashed lines have been obtained using correlations with only the scalar channel active, while the dash-dotted lines with correlations without the two tensor channels.

The results of Fig. 6 show the same behavior for each nucleus considered. In the nuclear interior, the correlated density distributions are smaller than the uncorrelated ones. We notice that the curves obtained with purely scalar correlations are the more distant ones from the uncorrelated re-

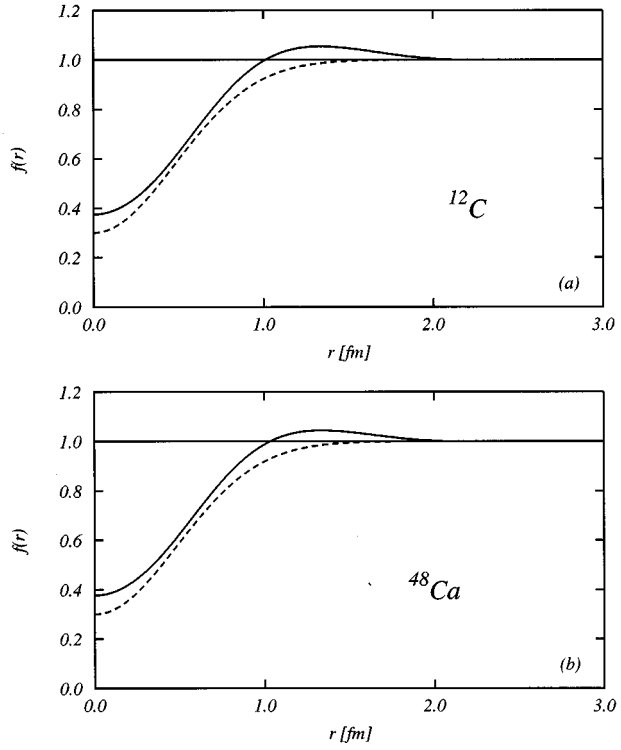

FIG. 3. Correlation functions used in the ^{12}C and ^{48}Ca calculation of Fig. 4. The dashed lines show the Gaussian correlations and the full lines the correlations obtained with a Euler minimization procedure.

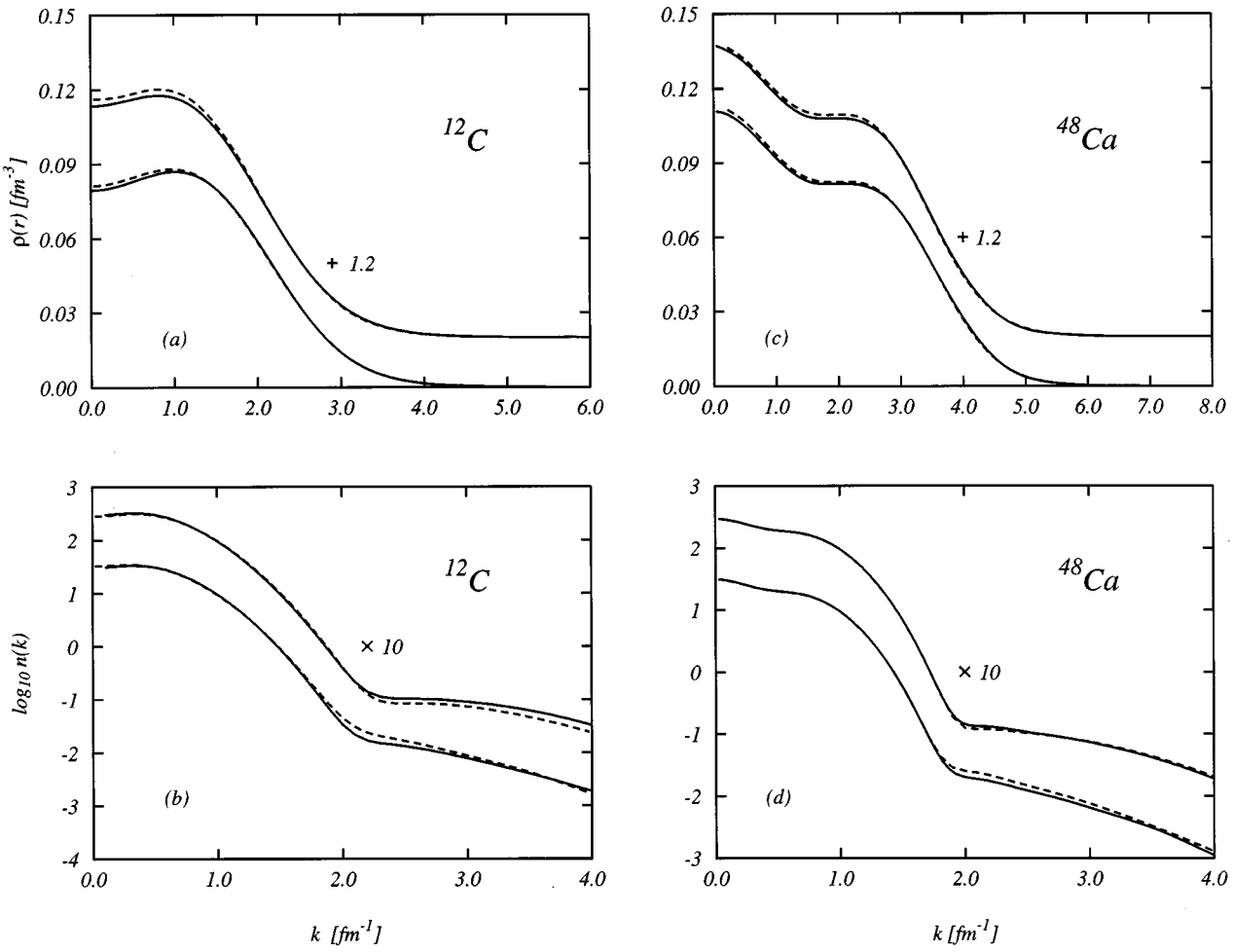

FIG. 4. Comparison between density (upper panels) and momentum distributions (lower panels) calculated with our model (dashed lines) and with a full FHNC calculation [10]. We have added a factor 1.2 to the densities calculated with the Euler correlations and we have multiplied the Euler momentum distributions by a factor 10.

sults. The inclusion of the other correlation channels reduces these differences.

The momentum distributions (Fig. 7) show a well-known behavior. Correlated and uncorrelated results are practically the same up to momentum values of about 1.8–2.0 fm^{-1}, but they clearly separate at higher values. The uncorrelated distributions descend very rapidly while the correlated distributions are an order of magnitude larger.

In Fig. 7 we observe that the full lines and dashed lines, obtained with correlations containing only the scalar term, are well separated in the high momentum region. On the contrary, the full and dash-dotted lines, the last ones obtained using correlations without the tensor channels differ only in a small momentum region around 2.0 fm^{-1}. This fact leads us to think that the effects of the tensor correlations are well localized in momentum space.

To better investigate this issue we have performed calculations of the momentum distributions using correlations with only the tensor channels active. The result for the ^{12}C nucleus is presented in Fig. 8 (dotted line) and is compared with the momentum distribution calculated with the full correlation (full line) and with that obtained with central and tensor terms only (dashed line).

We observe that the filling of the dip around 2 fm^{-1} is produced by the sum of the effects of the scalar and tensor components. The other central channels are responsible for the increase of the tail of the distribution at higher momentum values.

IV. CONCLUSIONS

We have developed a nuclear model to describe density and momentum distributions of doubly closed shell nuclei explicitly considering the short-range correlations.

This model is based upon the cluster expansion of the CBF theory, but it retains only the set of lowest order diagrams which allows for the conservation of the number of particles.

The model has been tested against the results obtained by finite nuclei FHNC calculations performed with the same inputs. The agreement between our results and those of the more elaborate theory is very good.

We have calculated momentum and density distributions of four doubly closed shell nuclei with state dependent correlations taken from nuclear matter FHNC calculations.

We found that the major effects of the correlations in both density and momentum distributions are produced by the scalar part of the correlations. The effect of the correlation

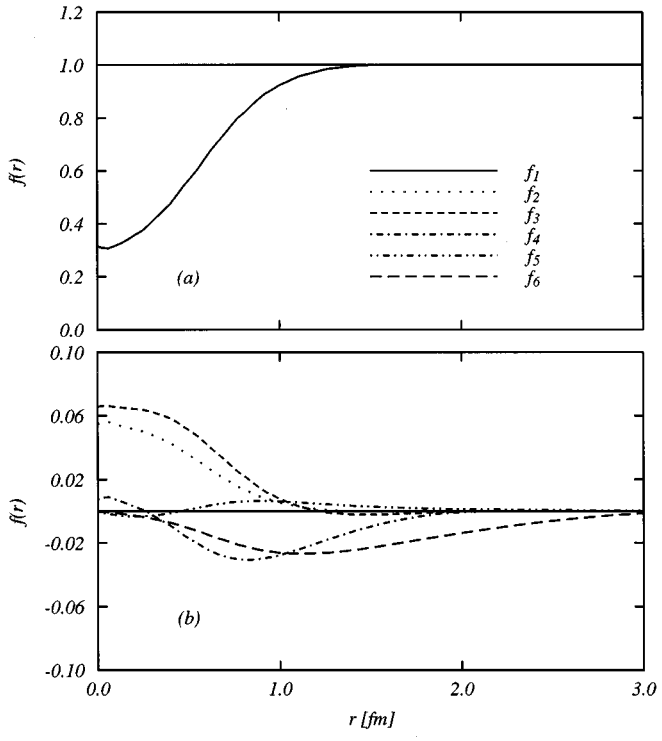

FIG. 5. State dependent correlation terms as a function of the interparticle distance [17]. See Eq. (8) for the meaning of the various lines.

functions used in these calculations is a general lowering of the density distributions in the interior region and an increasing of the momentum distribution at high momentum values.

The effect of the state dependent terms of the correlation on the density distribution is of opposite sign with respect to the effect of the scalar term only. The results obtained with the complete correlation are closer to the uncorrelated results than those obtained with the scalar term only. The situation is reversed in the momentum distribution case.

The tensor correlation term produces effects which seem to be rather localized in momentum space. In the momentum distributions, the presence of the tensor correlations is noticeable in a small momentum region around the point where the uncorrelated distributions separate from the correlated ones.

Before concluding we would like to make two comments about the limitations of the model with respect to FHNC calculations. A first limitation is of practical type. Contrary to what happens in the FHNC case, the numerical effort to perform our calculations grows rapidly with the number of single-particle states. This makes the calculation of the ^{208}Pb momentum distribution extremely heavy from the numerical point of view. The second limitation has a theoretical aspect common to all the models of the same kind. In the FHNC theory the correlation function and the s.p. basis are related through the nuclear Hamiltonian by the variational principle. In our model they are two different input parameters in principle arbitrary.

We have performed our calculations using reasonable s.p. bases and reasonable correlations. The s.p. bases have been taken from literature where their parameters have been fixed in order to reproduce some nuclear properties within a mean-field model. This could mean that some effects of the short-range correlations we would like to describe have already been averaged out by this procedure. The correlation function used has been obtained by a minimization procedure done in nuclear matter. We show in Fig. 3 that finite nuclei FHNC minimizations seems to prefer correlation functions with an overshooting in the region between 1 and 2 fm, but this is not the characteristic shown by the scalar term of the nuclear matter correlation function.

Because of these theoretical limitations, we believe that at the present stage the comparison of the results of our model with experimental data is not very meaningful. The validity of our work lies in the evaluation of the relative effects produced by the various correlation channels.

ACKNOWLEDGMENTS

This work was partially supported by the agreement CYCIT-INFN and the Junta de Andalucia.

APPENDIX

In this appendix we present the expressions of the equations used to calculate the diagrams of Fig. 1.

The functions G of Eqs. (22) are defined as

$$G1=(f_1+f_3)(g_1+g_3)+3(f_2+f_4)(g_2+g_4)+6(f_5+f_6)(g_5+g_6), \tag{A1}$$

$$G2=(f_1-f_3)(g_1-g_3)+3(f_2-f_4)(g_2-g_4)+6(f_5-f_6)(g_5-g_6), \tag{A2}$$

$$G3=f_3g_3+3f_4g_4+6f_6g_6, \tag{A3}$$

$$G4=(f_1+f_3)(g_1+g_3)+\left(\frac{1}{2}(f_2+f_4)-f_1-f_3\right)(g_2+g_4)+(f_2+f_4)\left(\frac{1}{2}(g_2+g_4)-g_1-g_3\right)+4(f_5+f_6)(g_5+g_6), \tag{A4}$$

$$G5=(f_1-f_2+f_3-f_4)(g_2+g_4)+(f_2+f_4)(g_1-g_2+g_3-g_4)+2(f_5+f_6)(g_5+g_6), \tag{A5}$$

$$G6=(f_1-f_3)(g_3-g_4)+(f_2-f_4)(5g_4-g_3)+4(f_5-f_6)g_6, \tag{A6}$$

$$G7=(f_2-f_4)g_3+(f_1-2f_2-f_3+2f_4)g_4+2(f_5-f_6)g_6, \tag{A7}$$

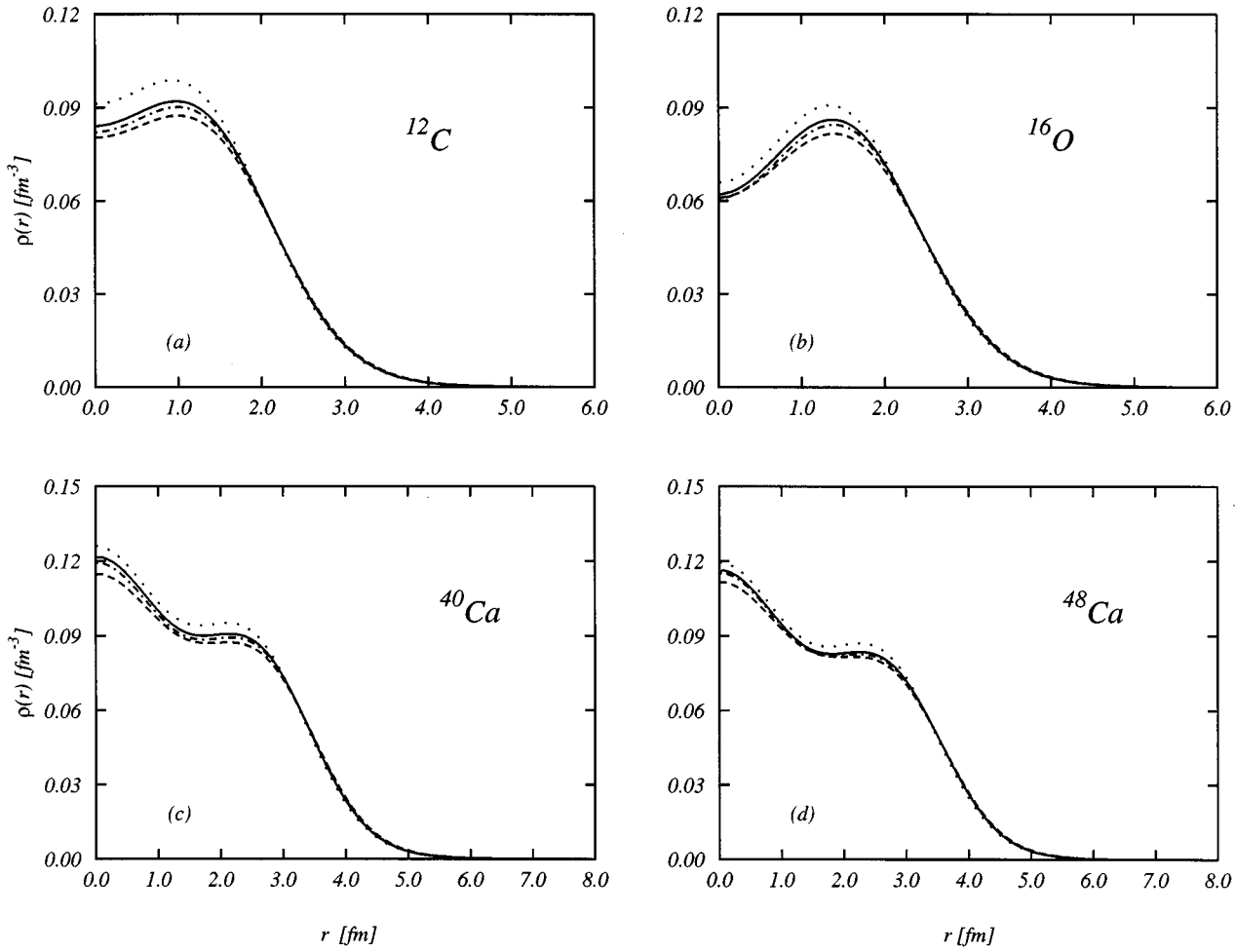

FIG. 6. Proton density distributions calculated with the correlation function of Fig. 5. The dotted lines show the uncorrelated results. The full lines have been obtained with the full correlations. The results of the calculations performed without the two tensor components of the correlations are shown by the dash-dotted lines, while the dashed lines show the results obtained with only the scalar term of the correlation (f_1).

$$G8=(f_3-f_4)(g_1-g_3)+(5f_4-f_3)(g_2-g_4)+4f_6(g_5-g_6), \tag{A8}$$

$$G9=f_3(g_2-g_4)+f_4(g_1-2g_2-g_3+2g_4)+2f_6(g_5-g_6). \tag{A9}$$

To describe the closed shell nuclei we have used a set of s.p. wave functions of the form

$$\phi^t_{nljm}(\mathbf{r}_i)=R^t_{nlj}(r_i)\sum_{\mu,s}\langle l\mu 1/2s|jm\rangle Y_{l\mu}(\Omega_i)\chi_s(i)\chi_t(i). \tag{A10}$$

In the above equation Ω_i indicates the angular coordinates, l and j the orbital and total angular momentum, respectively, $R_{nlj}(r)$ the radial part of the wave function, $Y_{l\mu}$ the spherical harmonic, and $\langle l\mu 1/2s|jm\rangle$ the Clebsch-Gordan coefficient.

In this basis the uncorrelated proton OBDM, the first term of Eq. (11) is

$$\rho^p_0(\mathbf{r}_1,\mathbf{r}_2)=\frac{1}{4\pi}\sum_{nlj} R^p_{nlj}(r_1)R^p_{nlj}(r_2)(2j+1)P_l(\cos\theta_{12}), \tag{A11}$$

where P_l is the Legendre polynomial and θ_{12} is the angle between $\mathbf{r}_1$ and $\mathbf{r}_2$.

The contribution of the other terms has been calculated using expression (A11) of the s.p. wave functions and performing a multipole expansion of each correlation function f_n and g_n of the G functions:

$$f_\alpha(\mathbf{r}_1,\mathbf{r}_2)=\sum_L f^\alpha_L(r_1,r_2)P_L(\cos\theta_{12}), \tag{A12}$$

where $\alpha=1,\ldots,6$.

The contribution of the diagrams A,B,C, and D has been calculated expanding in multipole each term composing expressions from (22) to (25). Each of these terms contains the product between the correlation functions f_n and g_n. In diagram A we found terms of the form:

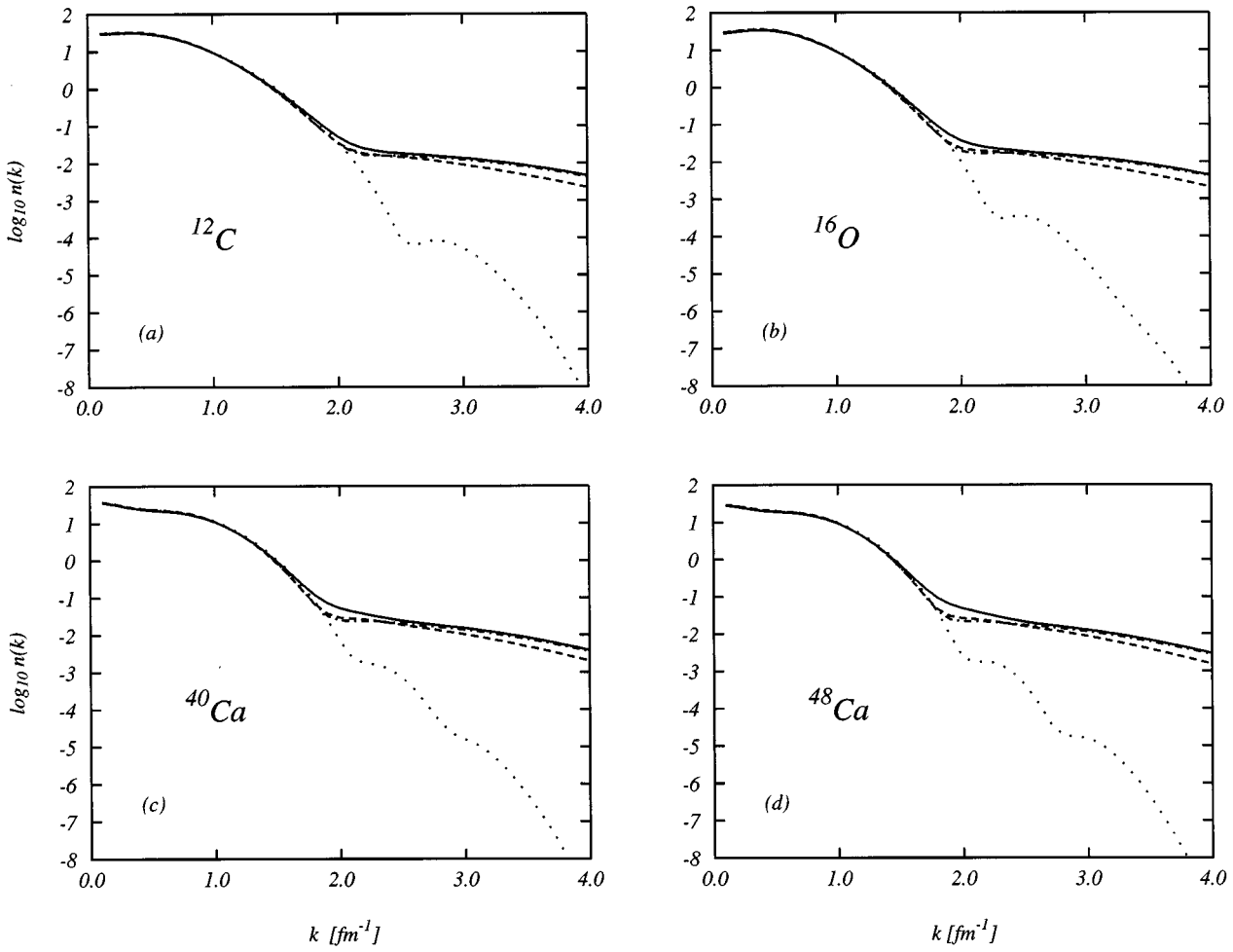

FIG. 7. Proton momentum distributions. The meaning of the various lines is the same as in Fig. 5.

$$\rho_0^{t_1}(\mathbf{r}_1,\mathbf{r}_1')\int d^3r_2\rho_0^{t_2}(r_2)f_\alpha(r_{12})g_\beta(r_{1'2})=\sum_{n_1,l_1,j_1}(2j_1+1)R^{t_1}_{n_1,l_1,j_1}(r_1)R^{t_1}_{n_1,l_1,j_1}(r_1')$$
$$\times\sum_{l_2,l_3}\frac{2l_3+1}{2l_2+1}\begin{pmatrix}l_1 & l_3 & l_2\\ 0 & 0 & 0\end{pmatrix}^2 P_{l_3}(\cos\theta_{11'})\int_0^\infty dr_2r_2^2\rho_0^{t_2}(r_2)f^\alpha_{l_2}(r_1,r_2)g^\beta_{l_2}(r_1',r_2). \tag{A13}$$

In diagram B we calculate terms of the form

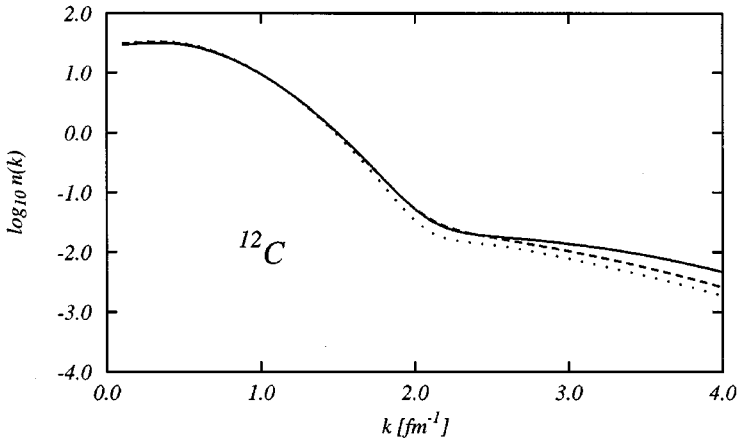

FIG. 8. Proton momentum distribution of ^{12}C. The full line corresponds to the full calculation (the same as in Fig. 7). The dotted line has been obtained using only the two tensor components of the correlation and the dashed line with the scalar plus tensor components.

$$\int d^3r_2\rho_0^{t_1}(\mathbf{r}_1,\mathbf{r}_2)\rho_0^{t_2}(\mathbf{r}_2,\mathbf{r}_1')f_\alpha(r_{12})g_\beta(r_{1'2})=\frac{1}{4\pi}\sum_{\substack{n_1,l_1,j_1\\n_2,l_2,j_2}}(2j_1+1)(2j_2+1)$$
$$\times R^{t_1}_{n_1,l_1,j_1}(r_1)R^{t_2}_{n_2,l_2,j_2}(r_1')\sum_{l_3,l_4,l_5}(2l_5+1)\begin{pmatrix}l_1&l_5&l_3\\0&0&0\end{pmatrix}^2\begin{pmatrix}l_2&l_5&l_4\\0&0&0\end{pmatrix}^2$$
$$\times\int_0^\infty dr_2r_2^2R^{t_1}_{n_1,l_1,j_1}(r_2)R^{t_2}_{n_2,l_2,j_2}(r_2)f^\alpha_{l_3}(r_1,r_2)g^\beta_{l_4}(r_1',r_2)\quad P_{l_5}(\cos\theta_{11'})\quad\text{(A14)}$$

and

$$\sum_{s_1,s_2}\int d^3r_2\rho_0^{s_1s_2t_1}(\mathbf{r}_1,\mathbf{r}_2)\rho_0^{s_2s_1t_2}(\mathbf{r}_2,\mathbf{r}_1')f_\alpha(r_{12})g_\beta(r_{1'2})$$
$$=-\frac{1}{4\pi}\sum_{\substack{n_1,l_1,j_1\\n_2,l_2,j_2}}\sqrt{(2l_1+1)(2l_2+1)}(2j_1+1)(2j_2+1)R^{t_1}_{n_1,l_1,j_1}(r_1)R^{t_2}_{n_2,l_2,j_2}(r_1')$$
$$\times\sum_{l_3,l_4,l_5,l_6}(-1)^{l_5-l_6}\frac{1+(-1)^{l_1+l_2+l_5}}{2}(2l_5+1)(2l_6+1)\times\int_0^\infty dr_2r_2^2R^{t_1}_{n_1,l_1,j_1}(r_2)R^{t_2}_{n_2,l_2,j_2}(r_2)f^\alpha_{l_3}(r_1,r_2)g^\beta_{l_4}(r_1',r_2)$$
$$\times\begin{pmatrix}j_2&j_1&l_5\\1/2&-1/2&0\end{pmatrix}\begin{pmatrix}l_3&l_5&l_4\\0&0&0\end{pmatrix}\begin{pmatrix}l_2&l_6&l_4\\0&0&0\end{pmatrix}\begin{pmatrix}l_1&l_6&l_3\\0&0&0\end{pmatrix}\begin{Bmatrix}l_1&l_2&l_5\\j_2&j_1&1/2\end{Bmatrix}\begin{Bmatrix}l_2&l_4&l_6\\l_3&l_1&l_5\end{Bmatrix}\quad P_{l_6}(\cos\theta_{11'})$$

In diagrams C and D the functions describing the correlations depend only on two radial coordinates, therefore we can perform the multipole expansion of their product. So we shall define

$$h_{\alpha\beta}(r_{23})=f_\alpha(r_{23})f_\beta(r_{23}).\qquad\text{(A15)}$$

In diagram C we obtain terms of the form

$$\sum_{s_1,s_2}\int d^3r_2d^3r_2\rho_0^{s_1s_2p}(\mathbf{r}_1,\mathbf{r}_2)\rho_0^{s_2s_1p}(\mathbf{r}_2,\mathbf{r}_1')\rho_0^t(r_3)h_{\alpha\beta}(r_{23})$$
$$=\sum_{\substack{n_1,l_1,j_1\\n_2}}(2j_1+1)R^p_{n_1,l_1,j_1}(r_1)R^p_{n_2,l_1,j_1}(r_1')\int_0^\infty dr_2r_2^2R^p_{n_1,l_1,j_1}(r_2)R^p_{n_2,l_1,j_1}(r_2)\int_0^\infty dr_3r_3^2\rho_0^t(r_3)h_0^{\alpha\beta}(r_2,r_3)P_{l_1}(\cos\theta_{11'}),\qquad\text{(A16)}$$

while diagram D we calculate terms of the form

$$\sum_{s_1,s_2}\int d^3r_2d^3r_3\rho_0^{s_1s_2p}(\mathbf{r}_1,\mathbf{r}_2)\rho_0^t(\mathbf{r}_2,\mathbf{r}_3)\rho_0^{s_2s_1p}(\mathbf{r}_3,\mathbf{r}_1')h_{\alpha\beta}(r_{23})$$
$$=\frac{1}{4\pi}\sum_{\substack{n_1,l_1,j_1\\n_2,l_2,j_2n_3}}(2j_1+1)(2j_2+1)R^p_{n_1,l_1,j_1}(r_1)R^p_{n_3,l_1,j_1}(r_1')P_{l_1}(\cos\theta_{11'})\times\sum_{l_4}\begin{pmatrix}l_1&l_2&l_4\\0&0&0\end{pmatrix}^2B(r_1,r_1')\qquad\text{(A17)}$$

and

$$\sum_{s_1,s_2,s_3}\int d^3r_2d^3r_3\rho_0^{s_1s_2p}(\mathbf{r}_1,\mathbf{r}_2)\rho_0^{s_2s_3t}(\mathbf{r}_2,\mathbf{r}_3)\rho_0^{s_3s_1p}(\mathbf{r}_3,\mathbf{r}_1')h_{\alpha\beta}(r_{23})$$
$$=\frac{1}{4\pi}\sum_{\substack{n_1,l_1,j_1\\n_2,l_2,j_2n_3}}(2j_1+1)(2j_2+1)R^p_{n_1,l_1,j_1}(r_1)R^p_{n_3,l_1,j_1}(r_1')P_{l_1}(\cos\theta_{11'})\sum_{l_4}\frac{1+(-1)^{l_1+l_2+l_4}}{2}\begin{pmatrix}j_2&j_1&l_4\\1/2&-1/2&0\end{pmatrix}^2B(r_1,r_1')$$

(A18)

where we have defined

$$B(r_1,r_1')=\int_0^\infty dr_2 r_2^2 R^p_{n_1,l_1,j_1}(r_2)R^t_{n_2,l_2,j_2}(r_2)\int_0^\infty dr_3 r_3^2 R^t_{n_2,l_2,j_2}(r_3)R^p_{n_3,l_1,j_1}(r_3)h_{l_4}^{\alpha\beta}(r_2,r_3). \tag{A19}$$

[1] J. M. Cavedon *et al.*, Phys. Rev. Lett. **49**, 978 (1982).

[2] E. N. M. Quint *et al.*, Phys. Rev. Lett. **57**, 186 (1986); E. N. M. Quint *et al.*, *ibid.* **58**, 1088 (1987).

[3] R. Jastrow, Phys. Rev. **98**, 1479 (1955).

[4] V. R. P. Pandharipande and R. B. Wiringa, Rev. Mod. Phys. **51**, 821 (1979); S. Rosati, in *From Nuclei to Particles*, Proceedings of the International School of Physics ''Enrico Fermi,'' Course LXXIX, edited by A. Molinari (North-Holland, Amsterdam, 1982).

[5] J. W. Clark, Prog. Part. Nucl. Phys. **2**, 89 (1979).

[6] V. R. Pandharipande, *Proceedings of Cargèse Summer School 1989*, Cargèse 1989, edited by J. Tran Tranh Van and J. Negele (Plenum Press, New York, 1990).

[7] S. C. Pieper, R. B. Wiringa, and V. R. Pandharipande, Phys. Rev. C **46**, 1741 (1992).

[8] G. Co', A. Fabrocini, S. Fantoni, and I. E. Lagaris, Nucl. Phys. **A549**, 439 (1992).

[9] G. Co', A. Fabrocini, and S. Fantoni, Nucl. Phys. **A568**, 73 (1994).

[10] F. Arias de Saavedra, G. Co', A. Fabrocini, and S. Fantoni, Nucl. Phys. **A605**, 359 (1996).

[11] F. C. Khanna, Phys. Rev. Lett. **20**, 871 (1968); W. J. Gerace, and D. A. Sparrow, Phys. Lett. **30B**, 71 (1969); C. Ciofi degli Atti, and N. M. Kabachnik, Phys. Rev. C **1**, 809 (1971).

[12] M. Gaudin, J. Gillespie, and G. Ripka, Nucl. Phys. **A176**, 237 (1971).

[13] O. Bohigas and S. Stringari, Phys. Lett. **95B**, 9 (1980); M. Dal Rì, S. Stringari, and O. Bohigas, Nucl. Phys. **A376**, 81 (1982); F. Dellagiacoma, G. Orlandini, and M. Traini, *ibid.* **A393**, 95 (1983); S. Stringari, M. Traini, and O. Bohigas, *ibid.* **A516**, 33 (1990).

[14] O. Benhar, C. Ciofi degli Atti, S. Liuti, and G. Salmè, Phys. Lett. B **177**, 135 (1986).

[15] M. V. Stoitsov, A. N. Antonov, and S. S. Dimitrova, Phys. Rev. C **47**, R455 (1993); **48**, 74 (1993); Z. Phys. A **345**, 359 (1993).

[16] G. Co', Nuovo Cimento A **108**, 623 (1995).

[17] R. B. Wiringa, V. Fiks, and A. Fabrocini, Phys. Rev. C **38**, 1010 (1988); A. Fabrocini (private communication).

[18] S. Fantoni and S. Rosati, Nucl. Phys. **A328**, 478 (1979).

[19] M. M. Renis, Tesi di Laurea, Università di Lecce, 1995.

[20] G. Co' and S. Krewald, Phys. Lett. **127B**, 145 (1984); G. Co', A. M. Lallena, and T. W. Donnelly, Nucl. Phys. **A469**, 684 (1987); J. E. Amaro and A. M. Lallena, *ibid.* **A537** 585 (1992).

[21] I. R. Afnan and Y. C. Tang, Phys. Rev. **175**, 1337 (1968).